

A Nonlinear Macromodel of Operational Amplifiers in the Frequency Domain

EDGAR SÁNCHEZ-SINENCIO, MEMBER, IEEE, AND MARIAN L. MAJEWSKI

Abstract—A nonlinear macromodel for integrated circuit operational amplifiers has been developed for frequency-domain analysis. The main difference between this macromodel and those previously reported in the literature is that this model considers the influence of frequency and amplitude on the transfer function of the operational amplifier. The macromodel also includes the slew-rate effect on the open-loop frequency response and output-voltage distortion computed from the Fourier coefficients. The benefits of the developed macromodel are demonstrated by several examples, showing that the simulation is in good agreement with the experimental results. One important application of this macromodel is suggested to be in the computation of the dynamic range of active filters.

I. INTRODUCTION

THE INTEGRATED CIRCUIT operational amplifier (OA) is the most popular and widely used of all linear circuits in the design and construction of equipment. When designing with OA's, the performance of these amplifiers is frequently assumed to be ideal. In many cases this assumption is not reasonable and the predicted performance differs substantially from reality. For instance, if an OA is overdriven by a large input signal, the output signal is distorted and is limited to a maximum rate of change called the slew rate. Under these circumstances, an improved analysis of real OA's is very necessary when designing electronic circuits containing OA's. However, if the OA is modeled on the device level, the conventional network analysis programs require a large memory, an efficient solution technique, and a high CPU time, with a consequent high cost. This paper presents a solution to this problem by using a reduced complex network topology which models the terminal performance by a comparatively smaller number of network elements. This model, termed a macromodel, results in a reduction in cost, required memory, and required CPU time.

There are two basic approaches for macromodeling. One approach consists of successively simplifying the circuitry of the OA and substituting the circuitry by simpler circuits with ideal elements. The other approach, called "buildup," consists in proposing a circuit configuration meeting certain external circuit specifications, without necessarily resembling the original circuitry.

Several OA macromodels have been developed and reported in the literature [1]–[5]. Boyle *et al.* [3] presented

a macromodel obtained by using a combination of the two techniques mentioned before. Weil and McNamee [1] developed a simple macromodel obtained by using the "buildup" technique. These two macromodels are quite adequate for transient analysis, although not sufficiently complete for many important applications in the frequency domain. The objective of developing the macromodel presented here is to consider the amplitude dependence caused by slew rate for the ac steady-state problem. The emphasis of our macromodel is on frequency-domain applications and not nonlinear transient operation where good macromodels [1]–[3] are already available. Our macromodel uses only the "buildup" technique and has been developed to take the slew rate into account when the OA is overdriven by a large input signal and when the output voltage is a function of the input voltage and frequency. The macromodel also considers the usual characteristics of the OA, such as common mode rejection ratio, input impedance, and voltage gain, all as functions of frequency, considering the first and second dominant poles together with the output impedance inductor-like behavior. One of the important applications of this OA macromodel is in computing the dynamic range of active filters, where a macromodel including most of the real behavior is needed.

A description of the macromodel is given in Section II, including the computation of component values for implementation of the model in a more general analysis program. Section III deals with examples and a discussion of the simulation programs including experimental results. Conclusions and future work are presented in Section IV.

II. A NONLINEAR LARGE-SIGNAL MACROMODEL

A *four-stage* model is developed for use with an ac nodal analysis program capable of handling VCCS's with complex gain. A block diagram of the model is given in Fig. 1. The model's construction method is based on the symmetrical case of the saturation characteristics of Fig. 2 where $|VIM_1| = |VIM_2| = |VIM|^1$ and $|IM_1| = |IM_2| = |IM|$. The input stage plays the role of modeling the differential- and common-mode input impedance, $Z_{idm}(\omega)$ and $Z_{icm}(\omega)$, respectively, as well as the common-mode rejection ratio $CMRR(\omega)$. The first intermediate stage

¹ $VIM(IM)$ is the maximum voltage (current) to the second stage, not to cause a distorted output voltage (current).

Manuscript received July 15, 1977; revised April 5, 1978. This work was supported by the Consejo Nacional de Ciencia y Tecnología de México.

The authors are with the Department of Electronics, Instituto Nacional de Astrofísica, Óptica y Electrónica, Puebla, Pue., Mexico.

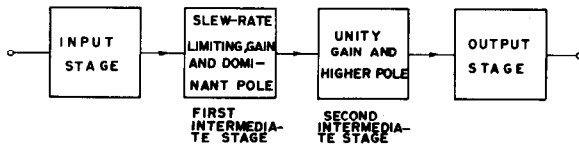


Fig. 1. Block diagram of the OA macromodel.

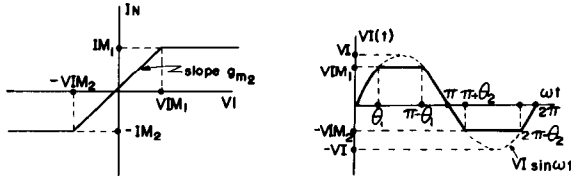
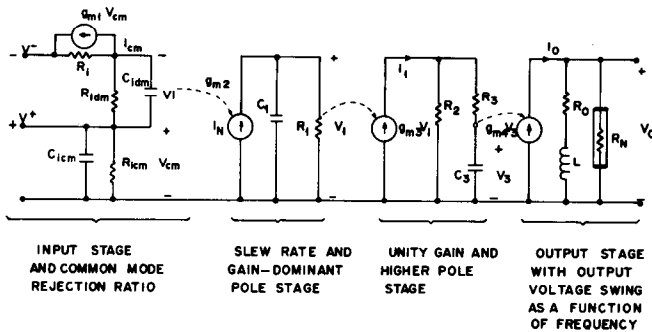
Fig. 2. Transfer characteristics including saturation characteristics of the VCCS, I_N of Fig. 3.

Fig. 3. Macromodel equivalent circuit.

takes into account the slew-rate characteristic S_r , as a function of the input voltage VI . This stage involves the differential-mode open-loop voltage gain A_{dm} , as well as the low-frequency dominant pole ω_1 . The saturation characteristics of the current source I_N are shown in Fig. 2(a) and serves to model the slew rate even when the OA is overdriven by a large input voltage VI . In this last case $VI > VIM$. This VI is computed by Fourier analysis and the slope,² g_{m2} of Fig. 2(a), is modified accordingly (more details are provided later). The second intermediate stage contains a unity gain connection with the first intermediate stage and the high-frequency dominant pole ω_2 . Finally, the output stage includes the output impedance with its inductor-like behavior and, in addition, considers the output voltage limiter. The current limiter is including in an earlier stage.

The proposed macromodel circuit is shown in Fig. 3. In the *first stage*, the effect of a finite frequency-dependent common-mode rejection ratio is referred to the input and modeled by the VCCS, called I_{cm} , where

$$I_{cm} = g_{m1} V_{cm} \quad (1)$$

with

²A piecewise-linear VCCS could be used to model the I - V characteristic of Fig. 2(a) if more accuracy is desired.

$$g_{m1} = \frac{1}{CMRR(\omega) \cdot R_i} \quad (2)$$

Observe that $CMRR(\omega)$ is frequency dependent and is expressed as

$$CMRR(\omega) = \frac{CMRR_0}{\left(1 + j \frac{f}{f_{CMRR}}\right)} \quad (3)$$

Since f_{CMRR} and R_{icm} are data obtained from the manufacturer's specifications, then C_{icm} can be computed as

$$C_{icm} = \frac{1}{2\pi R_{icm} f_{CMRR}} \quad (4)$$

The quantities R_{idm} and C_{idm} determine the differential input impedance Z_{idm} and these are also provided by the manufacturer. R_i is chosen such that

$$\frac{V_{cm}}{CMRR} = I_{cm} R_i \quad (5)$$

and

$$R_i \ll R_{idm}$$

In our model, we chose $R_i = 10 \Omega$. Analysis of this first stage gives the value of the internal differential voltage³ and the frequency dependence

$$VI = \frac{V^+ - V^- + g_{m1} V^+ R_i}{R_i + Z_{idm}} Z_{idm} \quad (6)$$

Now, in the *second stage*, using the saturation characteristics of Fig. 2(a) we have

$$g_{m2} = \frac{I_N}{VI} \quad (7)$$

and

$$I_N = \begin{cases} g_{m2} VI, & \text{for } |VI| \leq VIM \\ IM, & \text{for } |VI| > VIM. \end{cases} \quad (8)$$

Equation (8) involves both frequency and magnitude variation and must be evaluated under two conditions

$$|VI| \leq VIM \quad (CI)$$

$$|VI| > VIM. \quad (CII)$$

In the unsaturated case (CI) the parameters can be determined as follows.

Given S_r and the maximum output current swing,⁴ $I_{o, swing}$, from the maximum output voltage swing $|V_{o, swing}|$ provided by the manufacturer, we can determine the capacitor value C_1 . That is, since

$$I_{o, swing} = IM = S_r C_1 \quad (9)$$

³In fact, for $V^+ = V^-$, VI is not zero but still a small offset voltage.

⁴ $I_{o, swing} = |V_{o, swing}|/R_o$, where R_o is the output resistance.

TABLE I

VALUES OF $N_i(\cdot)$	NONSYMMETRICAL	SYMMETRICAL
N_0	$\frac{VI}{2\pi} 2(\cos \theta_2 - \cos \theta_1) - \frac{VIM_2}{VI} 2(\pi - 2\theta_2) + \frac{VIM_1}{VI} (\pi - 2\theta_1) $	_____
N_1	$\frac{VI}{\pi} \left[\sin^{-1} \left(\frac{VIM_1}{VI} \right) + \sin^{-1} \left(\frac{VIM_2}{VI} \right) + \frac{VIM_1}{VI} \sqrt{1 - \left(\frac{VIM_2}{VI} \right)^2} + \frac{VIM_2}{VI} \sqrt{1 - \left(\frac{VIM_1}{VI} \right)^2} \right]$	$\frac{2}{\pi} \left[\theta + \frac{VIM}{VI} \sqrt{1 - \left(\frac{VIM}{VI} \right)^2} \right]$
N_2	$\frac{2}{3} \frac{VI}{\pi} \left[\left(1 - \left(\frac{VIM_1}{VI} \right)^2 \right)^{3/2} - \left(1 - \left(\frac{VIM_2}{VI} \right)^2 \right)^{3/2} \right]$	_____
N_3	$\frac{VI}{\pi} \left[\frac{VIM_1}{VI} \left(\left(\frac{VIM_1}{VI} \right)^2 - 1 \right) \sqrt{1 - \left(\frac{VIM_2}{VI} \right)^2} + \frac{VIM_2}{VI} \left(\left(\frac{VIM_2}{VI} \right)^2 - 1 \right) \sqrt{1 - \left(\frac{VIM_1}{VI} \right)^2} \right]$	$\frac{2}{\pi} \frac{VIM}{VI} \left(\left(\frac{VIM}{VI} \right)^2 - 1 \right) \sqrt{1 - \left(\frac{VIM}{VI} \right)^2}$
N_4	$\frac{2}{15\pi} \left[\sqrt{1 - \left(\frac{VIM_1}{VI} \right)^2} \left(-9 \left(\frac{VIM_1}{VI} \right)^4 + 80.5 \left(\frac{VIM_1}{VI} \right)^2 + 31 \right) + \sqrt{1 - \left(\frac{VIM_2}{VI} \right)^2} \left(9 \left(\frac{VIM_2}{VI} \right)^4 - 80.5 \left(\frac{VIM_2}{VI} \right)^2 - 31 \right) \right]$	_____
N_5	$\frac{2}{15\pi} \left[\frac{VIM_1}{VI} \sqrt{1 - \left(\frac{VIM_1}{VI} \right)^2} \left(8 \left(\frac{VIM_1}{VI} \right)^4 - 11 \left(\frac{VIM_1}{VI} \right)^2 + 3 \right) + \frac{VIM_2}{VI} \sqrt{1 - \left(\frac{VIM_2}{VI} \right)^2} \left(8 \left(\frac{VIM_2}{VI} \right)^4 - 11 \left(\frac{VIM_2}{VI} \right)^2 + 3 \right) \right]$	$\frac{4}{15\pi} \frac{VIM}{VI} \sqrt{1 - \left(\frac{VIM}{VI} \right)^2} \left[8 \left(\frac{VIM}{VI} \right)^4 - 11 \left(\frac{VIM}{VI} \right)^2 + 3 \right]$
	$\theta_1 = \sin^{-1} \left(\frac{VIM_1}{VI} \right), \theta_2 = \sin^{-1} \left(\frac{VIM_2}{VI} \right)$	$\theta = \sin^{-1} \left(\frac{VIM}{VI} \right)$

then

$$C_1 = \frac{IM}{S_r} \tag{9a}$$

The lower dominant pole $\omega_1 = 2\pi f_3$ dB is known, and R_1 is directly given by

$$R_1 = \frac{1}{\omega_1 C_1} \tag{10}$$

The transconductance value g_{m2} is calculated from

$$g_{m2} = \frac{A_{dm}}{R_1} \tag{11}$$

VIM can be easily computed from

$$VIM = \frac{S_r}{A_{dm} \omega_1} = \frac{S_r C_1}{g_{m2}} \tag{12}$$

For the saturation case (CII), distortion occurs. This is shown pictorially in Fig. 2(b). A new value of g_{m2} is determined via Fourier analysis, this new value of g_{m2} includes not only the effects of the fundamental component but also those of the harmonics. We now determine the Fourier components, I_{Ni} , of the current source I_N . We have, in general,

$$I_{Ni} = \frac{1}{2\pi} \int_0^{2\pi} I_N(\omega t) \sin(n\omega t) d(\omega t), \tag{13}$$

$i, n = 0, 1, 2, \dots$

i) *Symmetric case:* Same as (13) with $i, n = 1, 3, 5, \dots$. By analogy from Fig. 2(b) for the current source I_N and

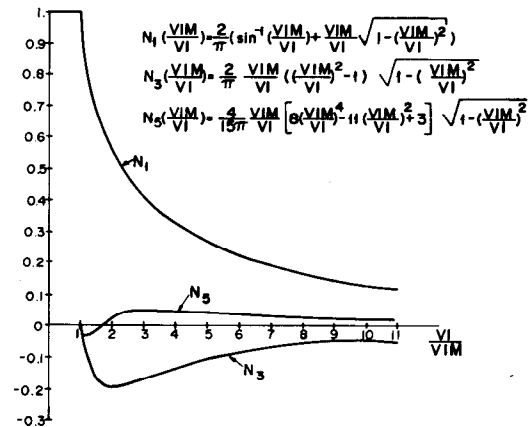


Fig. 4. Nonlinear characteristics of N_1, N_3, N_5 versus $|VI/VIM|$ for the symmetric case.

$\theta = \theta_1 = \theta_2$ (see Table I), we have

$$I_N(\omega t) = \begin{cases} IM, & \text{for } (\theta, \pi - \theta) \text{ and } (\pi + \theta, 2\pi - \theta) \\ g_{m2} VI \sin(\omega t), & \text{otherwise.} \end{cases}$$

Equation (13) can be written, in this case as

$$I_{Ni} = g_{m2} VI \cdot N_i \left(\frac{VIM}{VI} \right), \quad i = 1, 3, 5, \dots \tag{14}$$

The values of $N_i(VIM/VI)$ for the symmetric case are given in column two of Table I and are shown plotted in Fig. 4 as a function of $|VI/VIM|$.

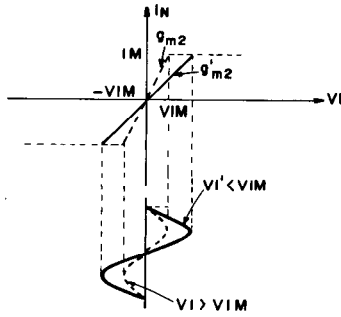


Fig. 5. Saturation characteristics of I_N when an OA is overdriven by a large input signal.

In a similar fashion, the components for V_I can be expressed as

$$V_I^i = V_I \cdot N_i \left(\frac{V_{IM}}{V_I} \right), \quad i = 1, 3, 5, \dots \quad (15)$$

Therefore, the output voltage of this second stage becomes

$$V_{out} = A_{dm1}(V_I' \sin \omega t) + A_{dm3}(V_I''' \sin 3\omega t) + A_{dm5}(V_I^v \sin 5\omega t) + \dots \quad (16)$$

It should be pointed out that V_I' , V_I''' , and V_I^v are not only functions of the input voltage amplitude but also of frequency in accordance with (6). A_{dm1} , A_{dm3} , and A_{dm5} are the gains at ω , 3ω , and 5ω , respectively.

Note that I_N is computed depending on conditions (CI) or (CII). The effect on the saturation characteristics is shown in Fig. 5, where for the fundamental component we can observe a compression effect on gain which is equivalent to decreasing the slope g_{m2} . Therefore, when $|V_I| > |V_{IM}|$, the linear g_{m2} becomes the nonlinear value g_{m2}^{non} , which is given by

$$g_{m2}^{non} = g_{m2} \left[N_1 \left(\frac{V_{IM}}{V_I} \right) + N_3 \left(\frac{V_{IM}}{V_I} \right) + N_5 \left(\frac{V_{IM}}{V_I} \right) + \dots \right] \quad (17)$$

and so

$$I_N = g_{m2}^{non} \cdot V_I. \quad (18)$$

Further simplifications of (17) is given later. Next we consider the more general case of nonsymmetry.

ii) *Nonsymmetric case:* In this case we have a dc component as well as odd and even components. That is, $I_{N_i}(\omega t)$ is given by (13), and its analogous voltage is shown in Fig. 2(b). The corresponding values of N_i are shown in column one of Table I, where θ_2 , θ_1 are defined. Also observe that for this nonsymmetric case, V_{out} for the second stage becomes

$$V_{out} = V_o + A_{dm1}(V_I' \sin \omega t) + A_{dm2}(V_I'' \cos 2\omega t) + A_{dm3}(V_I''' \sin 3\omega t) + A_{dm4}(V_I^{iv} \cos 4\omega t) + A_{dm5}(V_I^v \sin 5\omega t) + \dots$$

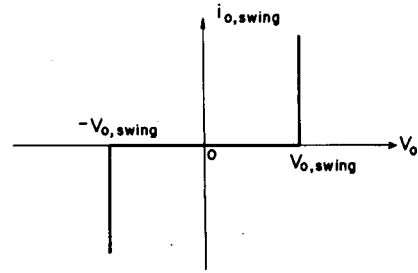


Fig. 6. V - I characteristic of the output nonlinear resistor R_N .

where

$$V_I^i = V_I \cdot N_i \left(\frac{V_{IM}}{V_I} \right), \quad i = 0, 1, 2, 3, \dots \quad (19)$$

Stage 3: Here the higher dominant pole,⁵ ω_2 , is simulated by $R_3 C_3$, where R_2 serves to connect the previous stage by unity gain with the restriction that $R_2 \ll R_3$. Here

$$C_3 = \frac{1}{\omega_2 R_3} \quad (20)$$

with R_3 and R_2 fixed. We also have

$$g_{m3} = \frac{1}{R_2}. \quad (21)$$

Stage 4: This models the output impedance with its inductor-like characteristics. The output impedance as well as R_o can be obtained from the manufacturer. We have immediately

$$\frac{R_o}{L} = \omega_o$$

or

$$L = \frac{R_o}{\omega_o}. \quad (22)$$

This stage is connected by unity gain to stage 3 through the VCCS g_{m4} , which is frequency dependent and has the value

$$g_{m4} = \frac{1}{R_o + j\omega L}. \quad (23)$$

This stage considers the output voltage swing with R_N [5], whose limiting values can be obtained from the manufacturer's data [7]. R_N can be specified by

$$R_N = \begin{cases} \infty, & \text{if } |V_{out}| \leq \max |V_{o, swing}| \\ 0, & \text{if } |V_{out}| > \max |V_{o, swing}| \end{cases}$$

where $V_{o, swing}$ is the maximum output voltage swing for large-signal gain, i.e., $|V_{o, swing}| = 10$ V [7]. The V - I characteristic of the output nonlinear resistor R_N is shown in Fig. 6. Observe that both limitations on output voltage and output current $I_{o, swing}$ have been considered in our

⁵In practice, for the 741 type, ω_2 is approximately between 2 and 7 MHz.

TABLE II
MODEL COMPONENTS AND AMPLIFIER PARAMETERS

Amplifier Parameters		
$A_{dm} = 2 \times 10^5$	$R_{idm} = 2 \times 10^6 \Omega$	$\omega_o = 2\pi \times 150 \times 10^3 \frac{\text{rad}}{\text{s}}$
$\omega_1 = 2\pi \times 5 \frac{\text{rad}}{\text{s}}$	$R_{icm} = 2 \times 10^9 \Omega$	$R_o = 75 \Omega$
$\omega_2 = 2\pi \times 2 \times 10^6 \frac{\text{rad}}{\text{s}}$	$C_{idm} = 1.4 \text{ pF}$	$S_T = 0.5 \text{ V}/\mu\text{s}$
$f_{CMRR} = 300 \text{ Hz}$	$CMRR_o = 31622.77$	$I_M = 133.3 \times 10^{-3} \text{ A}$
		$V_{omax} = \pm 10 \text{ V}$
Model Components		
$R_1 = 10 \Omega$	$g_{m2} = 1.67551 \text{ mhos}$	$L = 79.5 \mu\text{H}$
$C_{icm} = 0.265 \text{ pF}$	$R_2 = 10 \Omega$	$VIM = 79.5 \text{ mV}$
$R_1' = 0.11936 \text{ M}\Omega$	$R_3 = 1 \text{ k}\Omega$	$g_{m1} = 3.162 \times 10^6 \text{ mhos}$
$C_1 = 0.266 \mu\text{F}$	$C_3 = 79.6 \text{ pF}$	$g_{m3} = 0.1 \text{ mhos}$
	g_{m4} given by Eqn. (23)	

model. $I_{o, swing}$ was directly involved in (9) in the second stage and $V_{o, swing}$ in this output stage. An alternative method for the output limitations is to consider $I_{o, swing}$ in the output stage and $V_{o, swing}$ in the second stage.

The transfer function⁶ of the model involves more than two poles but basically exhibits two dominant poles.

For the case of an OA $\mu\text{A}741$ the values of the macromodel are shown in Table II. Observe that in the nonlinear region g_{m2} becomes g_{m2}^{non} as given in (17). The expression for g_{m2}^{non} can be simplified in the case when only the fundamental component (symmetric case) is considered. For this condition $N_1(VIM/VI)$ can be expressed simply as

$$N_1\left(\frac{VIM}{VI}\right) = \begin{cases} 1, & \left|\frac{VI}{VIM}\right| < 1.26 \\ 1.26 \frac{VIM}{VI}, & \left|\frac{VI}{VIM}\right| > 1.26. \end{cases} \quad (24)$$

The maximum error incurred when $N_1(\cdot)$, as given in Table I is substituted by (24), is less than 10 percent. Observe also that this simple form of $N_1(\cdot)$ permits us to reduce the computational effort. Furthermore, from Fig. 4, we note that $N_3(\cdot)$ is significantly smaller than $N_1(\cdot)$ and also significantly bigger than the rest of the harmonic components.

When the third harmonic is considered, an iterative scheme is required. A companion model of $I_N(3\omega t)$ for this harmonic is shown in Fig. 7 and obtained from a truncated Taylor series [5] where

$$B1 = -2g_{m2}VIM/\pi, \quad TT = \left|1 - \frac{B^2}{(x^k)^2}\right|^{1/2}$$

$$B2 = VIM^2, \quad X = VI.$$

⁶For instance, the transfer function, when V^+ is grounded, is given by

$$\frac{V_o}{V^-} \Big|_{V^+=0} = \frac{-g_{m2}g_{m3}R_1R_2R_{idm}}{(1+j\omega C_3(R_2+R_3))(1+j\omega R_1C_1)(R_{idm}+R_1(1+j\omega C_{idm}R_{idm}))}$$

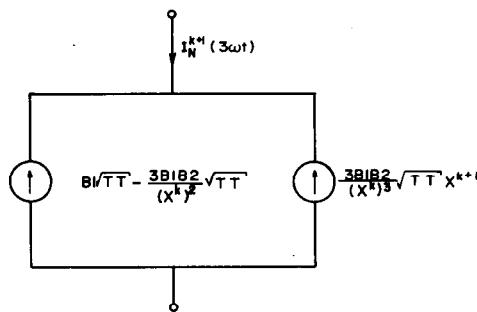


Fig. 7. Companion model of the third-harmonic component of $I_N(3\omega t)$. k is the iteration counter.

A stop criterion [5] for the computation of X is used, i.e., $|X^{k+1} - X^k| \leq \epsilon$ where ϵ is a prescribed acceptable error. Note that the third harmonic must be computed at a frequency three times greater than the operating frequency.

This companion model becomes specially useful when the frequency of operation is lower than the second pole of the OA, i.e., $3\omega < \omega_2$.

The assumption of the symmetry of I_N of Fig. 2 is acceptable in practice as shown in the following section. This assumption dramatically reduces the complexity of computation effort.

III. RESULTS OF SIMULATION AND EXPERIMENT

We present in this section three illustrative examples covering a wide range of applications.

i) Noninverting Configuration: The results of experiment together with the simulation are shown in Fig. 8 and show good agreement. Note that the results for the fundamental component agree with Allen's [8] with some variations since our macromodel uses a higher dominant pole and more real properties.

ii) Multiple-Feedback, Infinite Gain, Bandpass Filter: In order to further compare the response of the macromodel with the experimental results, we designed the active filter shown in Fig. 9 using our simulation instead of using the conventional approximate formulas [9]. In the simulation, the high central frequency, f_0 is 160 kHz. The OA employed exhibited the following parameters: $\omega_1 = 2\pi \times 5.182 \text{ rad/s}$, $A_{dm} = 1.81 \times 10^5$, and $\omega_2 = 2\pi \times 2.35 \times 10^6 \text{ rad/s}$. The results of simulation and experiment are shown in Fig. 10 where good agreement is seen. We note the importance of accurate knowledge of the parameter values of the OA especially in this range of frequencies where they play a dominant role. To illustrate this we show in Fig. 11 the effect of different values of A_{dm} , ω_1 , and ω_2 on the frequency response of the active filter of Fig. 10. The values used are as follows.

Case A:

$$\omega_1 = 2\pi \times 6.283 \text{ rad/s},$$

$$\omega_2 = 2\pi \times 2.3 \times 10^6 \text{ rad/s},$$

$$A_{dm} = 2.1 \times 10^5.$$

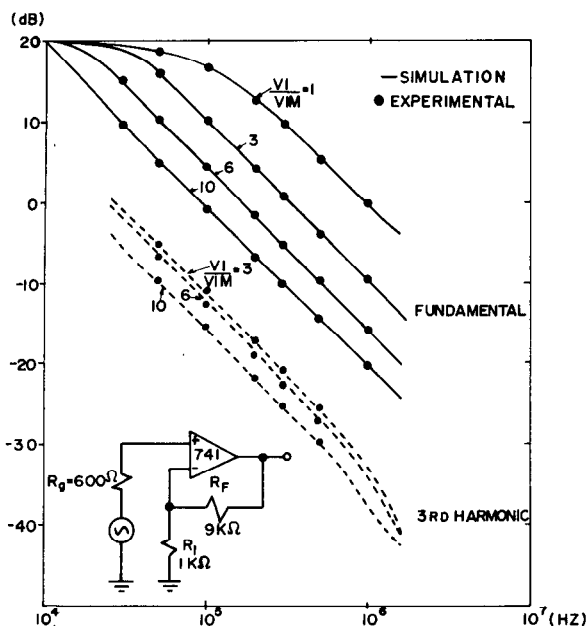


Fig. 8. Noninverting configuration. Simulation and experimental results.

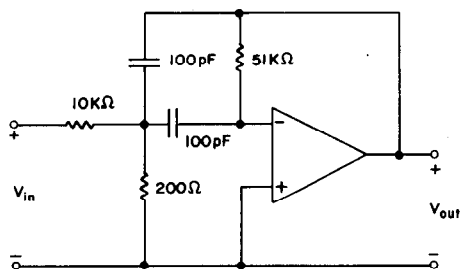


Fig. 9. RC-active bandpass filter.

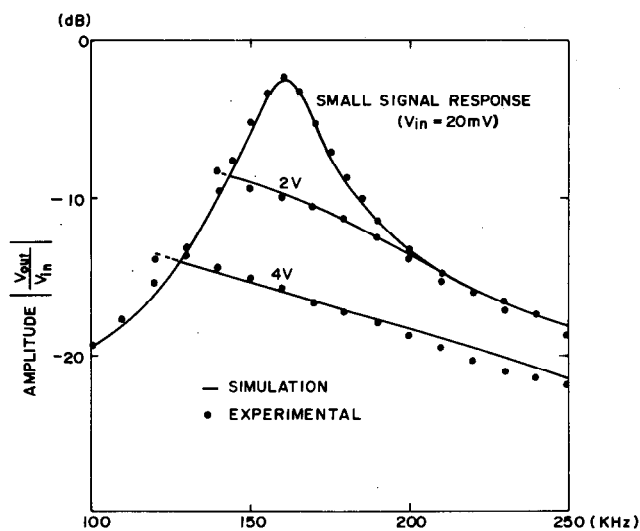


Fig. 10. Simulation and experimental results of the filter of Fig. 9.

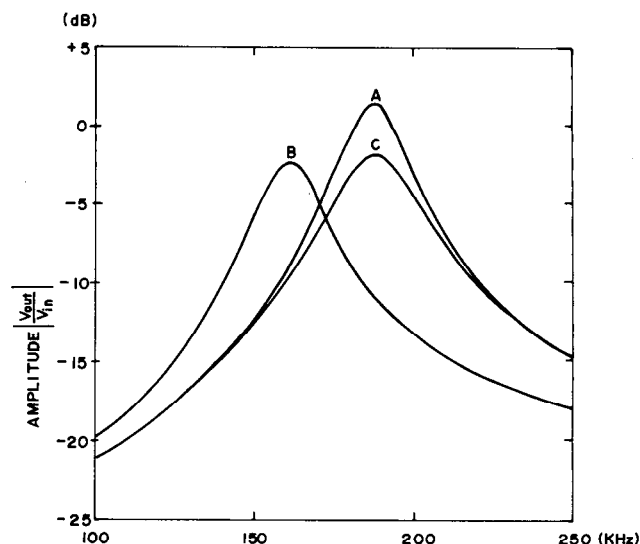


Fig. 11. Small-signal response of the filter of Fig. 9 for different parameter values of the OA.

Case B:

$$\omega_1 = 2\pi \times 5.182 \text{ rad/s,}$$

$$\omega_2 = 2\pi \times 2.3 \times 10^6 \text{ rad/s,}$$

$$A_{dm} = 1.81 \times 10^5.$$

Case C:

$$\omega_1 = 2\pi \times 6.283 \text{ rad/s,}$$

$$\omega_2 = 2\pi \times 7.3 \times 10^6 \text{ rad/s,}$$

$$A_{dm} = 2.1 \times 10^5.$$

The rest of the parameter values are the same as those given in Table II.

iii) *An R-Active Filter:* Finally, we present an example involving two OA's. This R-active filter [10] is shown in Fig. 12. The results of simulation and experiment shown in Fig. 13 again agree well. The data for the 741A are $\omega_1 = 2 \times 5.182 \text{ rad/s}$, $\omega_2 = 2.3 \times 2\pi \times 10^6 \text{ rad/s}$, and $A_{dm} = 1.81 \times 10^5$, for the 741B $\omega_1 = 2\pi \times 6.283 \text{ rad/s}$, $\omega_2 = 2.45 \times 2\pi \times 10^6 \text{ rad/s}$, and $A_{dm} = 2.1 \times 10^5$. The other parameter values are as given in Table II. Our macromodel does not include the hysteresis effect under large-signal conditions shown with dotted lines in Fig. 13. In the experimental results shown in Fig. 14 this hysteresis effect is exhibited. Curve 1 is obtained when the frequency is increased and this curve can be simulated by our model. Curve 2 of Fig. 14 is obtained when the frequency decreases. Observe from Figs. 13 and 14 that the jump frequency depends on the amplitude of the input. In Fig. 15 we show a picture of the experimental results, with an input signal of 0.8 V in the lower part and the distorted output signal in upper part, where the harmonics are added to the fundamental. The threshold for this filter before distortion corresponds to an input signal of 0.005 V.

The small-signal part of the macromodel has been successfully implemented in an HP2100A minicomputer

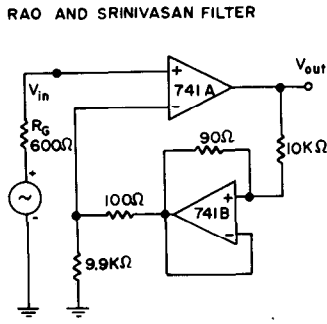


Fig. 12. A bandpass *R*-active filter.

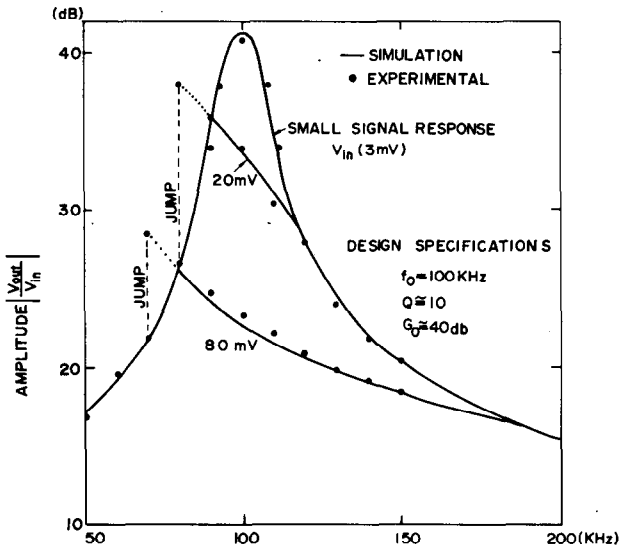


Fig. 13. Simulation and experimental results for different input signal amplitudes with the circuit of Fig. 12.

using sparse matrix techniques in a general linear frequency analysis program, named CAO II [11]. The computation time using this program for 72 frequency points with 16 nodes in the *R*-active filter (example iii) took 69 s.

The examples shown here were implemented for the large-signal part of the model using small special-purpose programs but not sparse matrix techniques. Computation of the fundamental using conventional solution techniques took 13 s for one frequency point, with the example iii). However, we should note that 88 percent of the entries of the admittance matrix used are zeroes. To compute the third harmonic for the noninverting configuration example took between 4 to 12 iterations.

IV. CONCLUSIONS AND FUTURE WORK

We have tackled the problem of developing an OA macromodel that can properly simulate slew-rate effects for the ac steady-state condition. This macromodel enables us to simulate the behavior of OA's for different frequencies with large input signals which is not possible with other existing macromodels [12]. That is, the output

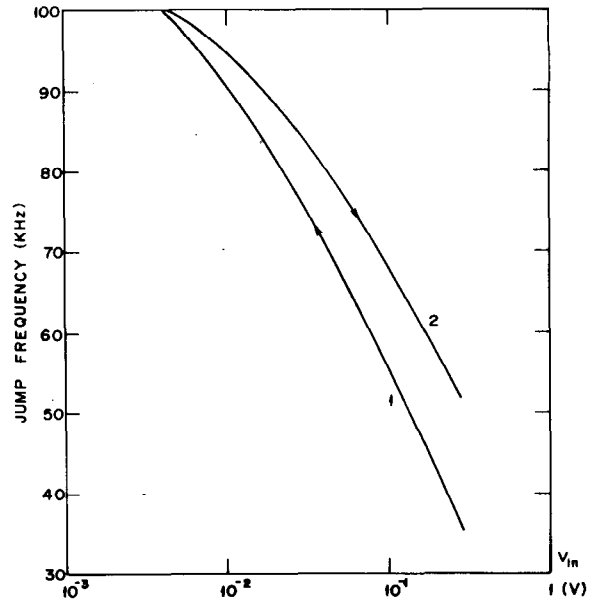


Fig. 14. The hysteresis effect showing the jump frequency around the central frequency of Fig. 12 versus input signal amplitude.

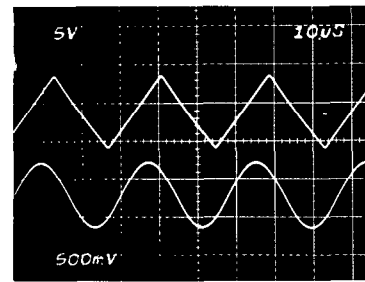


Fig. 15. An oscillogram of the experimental *R*-active filter.

signal depends on the amplitude of the input signal as well as the frequency of operation.

The complexity of the macromodel proposed is small, since it consists of only 12 passive elements, 3 linear VCCS's, and one nonlinear VCCS. This simplicity of the macromodel together with the fact that only current sources are employed makes the macromodel suitable for CAD. Furthermore, the values of the parameters used in the macromodel require knowledge of only the standard manufacturer's specifications [7].

Unfortunately, our macromodel makes no provision for the following commonly observed effects:

- a) variations of parameter values of the model versus supply voltage, or temperature variations;
- b) power dissipation [3];
- c) charge saturation (hysteresis) when the OA is overdriven by a large input signal.

Research is continuing to include this macromodel into a general nonlinear frequency analysis program and to study its applications for the design of limiters, mixers, detectors, and also to study the dynamic range of *RC*- and *R*-active filters.

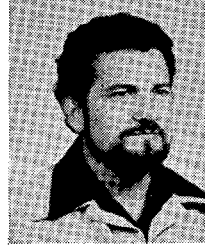
ACKNOWLEDGMENT

The authors wish to thank the reviewers who offered useful and constructive comments. Technical discussions with Prof. T. N. Trick, and Prof. P. E. Allen are gratefully acknowledged.

REFERENCES

- [1] P. Weil and L. P. McNamee, "A nonlinear macromodel for operational amplifiers," presented at the 8th Asilomar Conf. on Circuits, Systems and Computers, Pacific Grove, CA, Dec. 3-5, 1974.
- [2] M. Glesner and C. Weisang, "Computer aided macromodeling of integrated circuit operational amplifiers," in *IEEE Proc. ISCAS/76*, pp. 255-258, 1976.
- [3] G. R. Boyle, B. M. Cohn, D. O. Pederson, and J. E. Solomon, "Macromodeling of integrated circuit operational amplifiers," *IEEE J. Solid-State Circuits*, vol. SC-9, pp. 353-363, Dec. 1974.
- [4] D. H. Treleaven and F. N. Trofimenkoff, "Modeling operational amplifier for computer-aided circuit analysis," *IEEE Trans. Circuit Theory (Corresp.)*, vol. CT-18, pp. 205-207, Jan. 1971.
- [5] L. O. Chua and P. M. Lin, *Computer-Aided Analysis of Electronic Circuits: Algorithms and Computational Techniques*. Englewood Cliffs, NJ: Prentice-Hall, 1975.
- [6] J. E. Solomon, "The monolithic op. amp.: A tutorial study," *IEEE J. Solid-State Circuits*, vol. SC-9, pp. 314-332, Dec. 1974.
- [7] *Linear Integrated Circuits Data Book*, Fairchild Corp., 1976.
- [8] P. E. Allen, "Slew induced distortion in operational amplifiers," *IEEE J. Solid-State Circuits*, vol. SC-12, pp. 39-44, Feb. 1977.
- [9] D. S. Stout and M. Kaufman, *Handbook of Operational Amplifier Circuit Design*. New York: McGraw-Hill, 1976, ch. 12.
- [10] K. R. Rao and S. Srinivasan, "Low sensitivity active filters using the operational amplifier pole," *IEEE Trans. Circuits Syst.*, vol. CAS-21, pp. 260-262, Mar. 1974.
- [11] E. F. Dryere, E. Sánchez-Sinencio, and W. Chait, "A sparse matrix solution for minicomputer-aided network analysis," in *20th Midwest Symposium on Circuits and Systems*, pp. 617-621, Aug. 1977 (Ref. 17).

- [12] A. E. Ruehli, N. B. Rabbat, and H. Y. Hsieh, "Research report on macromodeling an approach for analyzing large scale circuits," IBM, Report RC 6789, 1977, 23 pages.



Edgar Sánchez-Sinencio (S'72-M'74) was born in Mexico City, Mexico, on October 27, 1944. He received the degree in communications and electronic engineering (professional degree) from the National Polytechnic Institute of Mexico, Mexico City, in 1966, and the M.S. and Ph.D. degrees from Stanford University, Stanford, in 1970, and from the University of Illinois at Champaign-Urbana, in 1973, respectively.

He did an industrial postdoctoral with the Central Research Laboratories, Nippon Electric Company, Ltd., Kawasaki, Japan. Since 1975 he has been with the Department of Electronics at the Instituto Nacional de Astrofísica, Óptica y Electrónica, Puebla, Mexico, where he is currently Professor and Head of the Department. His research interests include active networks, analog sampled data recursive filters, and digital processing of signals.

Marian L. Majewski, photograph and biography not available at the time of publication.

Sufficient Conditions for the Nonexistence of Limit Cycles in Two-Dimensional Digital Filters

N. G. EL-AGIZI AND MOUSTAFA M. FAHMY, SENIOR MEMBER, IEEE

Abstract—The stability of the two classes of two-dimensional digital filters defined by

$$F1: x_{i+1,j+1} = Q_R[ax_{i+1,j} + bx_{i,j+1} + cx_{i,j}]$$

and

$$F2: x_{i+1,j+1} = Q_R[ax_{i+1,j}] + Q_R[bx_{i,j+1}]$$

is studied. Here Q_R is the rounding operator, and fixed-point arithmetic is used. Sufficient conditions for the stability of $F1$ and necessary and sufficient conditions for the stability of $F2$ are derived. For the more general case of higher order two-dimensional (2-D) digital filters, sufficient conditions for the nonexistence of separable 2-D limit cycles are derived by extending the results of Claassen *et al.* [1].

Manuscript received March 9, 1978; revised September 20, 1978. This work has been partially supported by the Natural Sciences and Engineering Research Council of Canada under Grant A4149.

The authors are with the Department of Electrical Engineering, Queen's University, Kingston, Ont. K7L 3N6, Canada.

I. INTRODUCTION

LIMIT CYCLES in two-dimensional (2-D) digital filters have been considered before in [2]-[4]. Due to the difficulties involved in studying limit cycles, the previous authors restricted their studies to specific cases of first-, [2], and a special case of second-, [3], [4], order sections. Here, we are going to consider the two classes of 2-D digital filters defined by

$$F1: x_{i+1,j+1} = Q_R[ax_{i+1,j} + bx_{i,j+1} + cx_{i,j}]$$

and

$$F2: x_{i+1,j+1} = Q_R[ax_{i+1,j}] + Q_R[bx_{i,j+1}]$$

where Q_R is the rounding operator under fixed-point arithmetic. The realizations of $F1$ and $F2$ are shown in Fig. 1. Two theorems are proved. Theorem 1 gives